Nuclear Instruments and Methods in Physics Research B 394 (2017) 61–66

Contents lists available at ScienceDirect

Nuclear Instruments and Methods in Physics Research B

journal homepage: www.elsevier.com/locate/nimb

Correlation between ferromagnetism and the concentration of interfacial defects in multiferroic $Bi_7Fe_{2.75}Co_{0.25}Ti_3O_{21}$ studied by positron annihilation

W.N. Ge [a,b,1], X.N. Li [c,1], J.P. Xu [a,b], S.J. Huang [d], J.D. Liu [a,b], Z. Zhu [c], Z.P. Fu [c], Y.L. Lu [c,*], B.J. Ye [a,b,*]

[a] State Key Laboratory of Particle Detection and Electronics, University of Science and Technology of China, Hefei 230026, People's Republic of China
[b] Department of Modern Physics, University of Science and Technology of China, Hefei 230026, People's Republic of China
[c] CAS Key Laboratory of Materials for Energy Conversion, Department of Materials Science and Engineering, University of Science and Technology of China, Hefei 230026, People's Republic of China
[d] Zhejiang University of Water Resources and Electric Power, Hangzhou 310018, People's Republic of China

ARTICLE INFO

Article history:
Received 9 January 2016
Received in revised form 9 March 2016
Accepted 20 December 2016
Available online 3 January 2017

Keywords:
Interfacial defects
Saturation magnetization
Annealing
Multiferroic materials

ABSTRACT

This paper investigated the effect of the annealing temperature on the interfacial defects and the magnetization of a single-phase multiferroic $Bi_7Fe_{2.75}Co_{0.25}Ti_3O_{21}$. With the increase of annealing temperature, the average thickness of the nonaplates increased from 80 to 180 nm. But the magnetic property measurement shows that the saturation magnetization gradually decreases with the increase of the annealing temperature correspondingly. Positron annihilation measurements reveal that the interfacial defects disappear obviously when the annealing temperature increased, which is found to agree well with the variation of saturation magnetization. The results suggest that with the higher concentration of interfacial defects may bring about higher saturation magnetization for the Aurivillius phase material, opening a window to improve the magnetic performance through controlling the concentration of interfacial defects.

1. Introduction

Multiferroic materials have attracted much attention because of their importance to significant technological promise in the multistate memory, energy harvesting, photocatalysis, et al. [1–5]. The most studied single phase multiferroic $BiFeO_3$ was limited by its weak performance, including its antiferromagnetic (AFM) nature at room temperature (RT) [6]. The layered Bi-containing oxides based on Aurivillius phase with the general formula of $Bi_4Bi_{n-3}Fe_{n-3}Ti_3O_{3n+3}$ (BFTO, n denotes the number of perovskite layers) have been likely known as another promising candidates to exhibit single-phase multiferroics [7–9]. Layered Aurivillius phase materials have the crystalline structure that is an alternation of perovskite-like layers with the composition of $(A_{n-1}B_nO_{3n+1})^{2-}$ and fluorite-like layers of $(Bi_2O_2)^{2+}$. A two-dimensional (2D) crystalline atomic structure model of the BFTO (n = 6) is shown in Fig. 1. In this figure we can see that 6 layers of perovskites composed of 6-coordinated Ti and Fe ions are sandwiched by two fluorite-like $(Bi_2O_2)^{2+}$ layers. Compared with famous multiferroic $BiFeO_3$, the most advantage of Aurivillius phase is that it could be widely modulated using versatile dopants as well as by changing the layer number, n. For instance, by doping Co into the Aurivillius lattices ($Bi_5FeTi_3O_{15}$, n = 4; $Bi_7Fe_3Ti_3O_{21}$, m = 6), ferroelectricity and ferromagnetism have been dramatically improved and are successfully brought to RT from very low temperature [10]. Not long ago we have fabricated highly grain-oriented $Bi_7Fe_{3-x}Co_xTi_3O_{21}$ ceramic which presented further enhanced magnetization [11]. Great efforts made to realize substantial RT multiferroic and magnetoelectric properties, especially to improve the ferromagnetic performances actually raise a question regarding what caused the enhancement of the magnetic performance and how can we take advantage of the factors to get a further improvement. Yet, there is no theoretical study to clearly verify the magnetic enhancement mechanism of versatile Aurivillius so far, which is urgent to be intensively studied.

It is already well known that vacancy defects are playing a major role in determining room temperature magnetic property

* Corresponding authors at: State Key Laboratory of Particle Detection and Electronics, University of Science and Technology of China, Hefei 230026, People's Republic of China (B.J. Ye). CAS Key Laboratory of Materials for Energy Conversion, Department of Materials Science and Engineering, University of Science and Technology of China, Heifei 230026, People's Republic of China (Y.L. Lu).
E-mail addresses: yllu@ustc.edu.cn (Y.L. Lu), bjye@ustc.edu.cn (B.J. Ye).
[1] W.N. Ge and X.N. Li contributed equally to this work.

http://dx.doi.org/10.1016/j.nimb.2016.12.036
0168-583X/

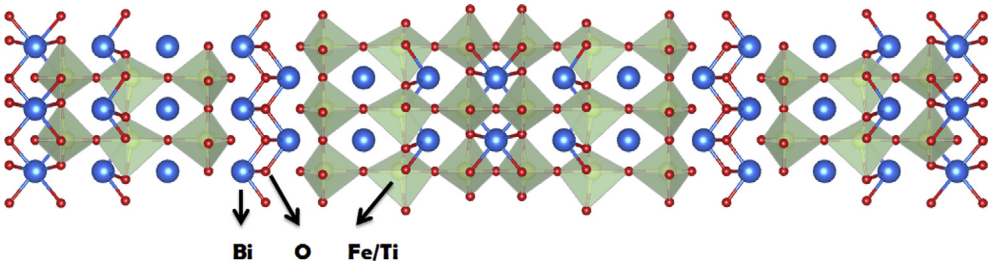

Fig. 1. The 2D atomic structure of the un-substituted $Bi_7Fe_3Ti_3O_{21}$.

of different oxides (e.g., $BaTiO_3$, ZnO, MgO, TiO_2, SnO etc.) [12–15]. Besides, the magnetism in some nanoparticles has been suggested probably originates from cation or anion vacancies at the surfaces [16,17]. It was also reported that in nanomaterials the structure of grain boundaries has neither long-range nor short-rangmke order [18]. Therefore the interfaces of nanocrystalline materials are rich of defects, which may have a special influence on the ferromagnetism of materials. So these interfacial defects deserve to be specifically investigated to find their correlation with the ferromagnetism.

Positron annihilation spectroscopy (PAS), which is highly sensitive to the change in properties of structural defects, has been employed to characterize these defects [19]. Positrons are trapped effectively by vacancy-type defects due to the Coulomb repulsion from the positron and positive ion cores. The two most used methods with positron annihilation are the positron annihilation lifetime spectroscopy (PALS) and the coincident Doppler-broadening spectroscopy (CDBS), which are very efficient in giving important information such as the size and concentrations of the vacancy defects, determining their charge states and so on [20].

Positron annihilation spectroscopy is particularly useful for the investigation of the interfacial defects in nanomaterials. This is because that the mean diffusion length of the thermalized positrons is longer than the grain size, which means that almost all the thermalized positrons would diffuse out to the grain surfaces and annihilate from there [21]. Therefore the effective grain boundary is magnified and the sensitivity of positrons to interfacial defects is greatly enhanced. Schaefer et al. [22] first reported positron annihilation study of the defects in Fe nanocrystals. Later several works about PAS studies in various nanomaterials were published [23–27]. In this paper, we studied the $Bi_7Fe_{2.75}Co_{0.25}Ti_3O_{21}$ samples which were treated with different annealing temperatures, so that we can investigate the effect of thermal treatment on the interfacial defects and the magnetization.

2. Experiment

The $Bi_7Fe_{2.75}Co_{0.25}Ti_3O_{21}$ (BFCTO) ceramic was prepared following the standard hydrothermal method reported in Ref. [11]. The obtained powders were pressed under a static pressure of about 5 MPa for 2 min at room temperature to get pellets in disk shape. The pellets have a diameter of 10 mm and a thickness of 1.5 mm. Then they were isochronally annealed at different temperatures (500, 650 and 800 °C) for 2 h at normal atmosphere. Finally, the samples were down to the room temperature naturally. For convenience, the samples with different annealing temperatures of 500 °C, 650 °C, 800 °C and the non-annealed sample are named as BFCTO-500, BFCTO-650, BFCTO-800 and BFCTO-RT, respectively.

The purity and crystallinity of all the samples were investigated using powder X-ray diffraction (XRD) with Cu-Kα radiation (Rigaku-TTR III). Morphology and nanoplate size were analyzed by scanning electron microscopy (SEM, JSM-6700F).Scanning transmission electron microscope (STEM) and elemental mapping were conducted with a field-emission transmission electron microscope (FETEM, JEOL JEM-2100F) equipped with an energy dispersive X-ray spectroscopy (EDS). Magnetic properties were characterized by the vibrating sample magnetometer (VSM) option of the Quantum Design physical property measurement system (PPMS) (Quantum Design, USA). Thermo-magneto-gravimetric (TMG) measurement was realized by thermo-gravimetric analysis and application of a magnetic field of 200 Oe (TGA Q5000IR, USA).

The positron lifetime spectroscopy (PALS) used plastic scintillator coupled with photomultiplier tubes as detectors and was measured with a fast-slow coincidence system which had a resolution of 230 ps. A 40 μCi ^{22}Na source of positron was sandwiched between two pieces of identical samples and each spectrum contained total counts of 2×10^6 to ensure the repeatability of the measurements. The coincidence Doppler broadening spectroscopy (CDBS) was measured using two HPGe detectors which had 1.5 keV energy resolutions at the energy of 511 keV. The source intensity is 30 μCi and the counting rate approximately 100 cps, each CDBS spectrum was collected with a total count over 8×10^6.

3. Results and discussion

3.1. Structures of the samples BFCTO

To study the crystallinity and the purity of the nanograins, four samples were subjected to XRD measurements. The XRD patterns of all BFCTO samples were shown in Fig. 2. From the figure we can see that all the observed peaks can be indexed to the Aurivillius structure of BFTO (n = 6, with a space group of Fm2 (42), JCPDS 54-1044) and no phase transition was observed. XRD patterns confirmed that all the samples were single phase with the Aurivillius structure. The SEM images of the BFCTO samples are shown in Fig. 3. By the multiple averaging measurements we can get that the average thickness of the nonaplates is about 80, 140 and 180 nm, respectively, which increases with the increase of the annealing temperature.

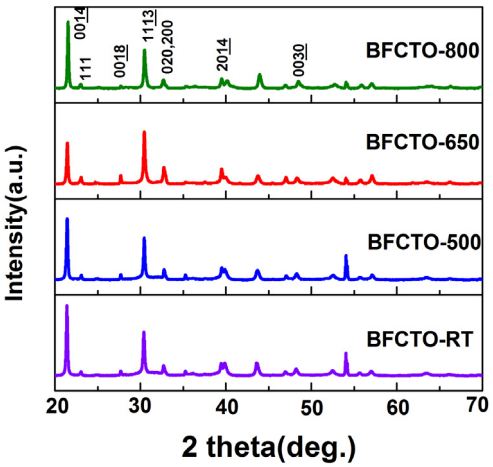

Fig. 2. XRD spectra of the BFCTO samples.

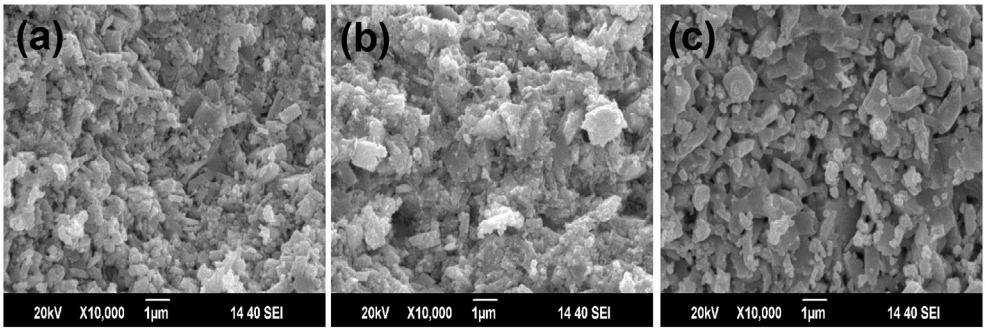

Fig. 3. SEM images of as-prepared BFCTO samples with different annealing temperatures: (a) BFCTO-500, (b) BFCTO-650 and (c) BFCTO-800, respectively.

3.2. Positron annihilation measurements

Positron lifetime spectra were measured for BFCTO samples annealed at different temperatures. All the lifetime spectra were evaluated to two lifetime components. Table 1 shows these two positron lifetime components τ_1 andτ_2, and it also gives the relative intensity I_2 and the mean lifetimes which calculated using the intensities as weight functions. These results reveal useful information about the defect structure of the BFCTO samples.

The shorter lifetime component (τ_1) is generally attributed to the free annihilation of positrons in defect-free crystal. However, smaller vacancies (like monovacancies, etc.) may be mixed with τ_1 in disordered systems, which will decrease the average electron density and increase the value of

τ_1 [28,29]. From the Table 1 we can see that the short lifetime component τ_1 of the sample BFCTO-RT is 233 ps, and it remains almost constant at 239.9 ps after annealing up to 500 °C, then the value obviously decreases to around 220 ps after annealing at 650 and 800 °C, which indicates that part of the monovacancies disappear. As for the longer lifetime τ_2, it arises from positrons trapped by larger size defects such as divacancies or vacancy clusters. An increase of τ_2 with initial annealing up to ~500 °C has been found from Table 1, which means some larger size vacancy clusters appear on the grain surfaces. It's because that the intragrain monovacancies migrate towards the grain surfaces when they obtain thermal energy, and part of these monovacancies agglomerate to form larger size vacancy [30]. A decrease of τ_2 is observed as the annealing temperature increases from 500 °C to 800 °C. Combined with the images of SEM, we can also say that the lifetime τ_2 decreases as the grain sizes become larger. Many articles have given the similar conclusion that the lifetime of positron annihilating in the diffused vacancy clusters on the grain surfaces will decrease with the grain sizes increasing [31,32]. So the result we measured is consistent with the general trend in nanocrystalline samples. Model analysis has already shown that the excess free volume associated with the atoms on the grain surfaces will decrease asymptotically with increasing grain sizes and hence the average vacancy size and the positron lifetime of τ_2 will also decrease [32]. All the monovacancies and vacancy clusters revealed by τ_1 and τ_2 are most located at the grain boundary region and called interfacial defects in this work.

Due to the complexity of the vacancies in the samples, only depending on the decomposition result of the positron lifetime spectra is not enough, we also rely on the mean positron lifetime. The mean positron lifetime $\tau_m = (\tau_1 I_1 + \tau_2 I_2)/(I_1 + I_2)$ could present an overall reflection on the defect traps and provide the details of the defect distribution in the samples. It is showed that the value of τ_m gradually decreases with the increase of annealing temperature, which indicates that the interfacial defects in the grain boundary region disappear slowly with the increase of annealing temperature. As a further support to the analysis of defects above, we also give the S-parameter which derived from the CDBS. The S-parameter reflects the annihilations with the low-momentum valence electrons, that is to say, it can reflect the relative concentrations of defects. Fig. 4 shows the S-parameter as a function of the annealing temperature for the BFCTO samples. From the figure we can see that with the increase of the annealing temperature, the S-parameter obviously decreases. Therefore, no matter in the PALS measurement or in the CDB measurement, we can obtain the same conclusion about the changing process of the defects, i.e., the interfacial defects disappear gradually with the increase of annealing temperature.

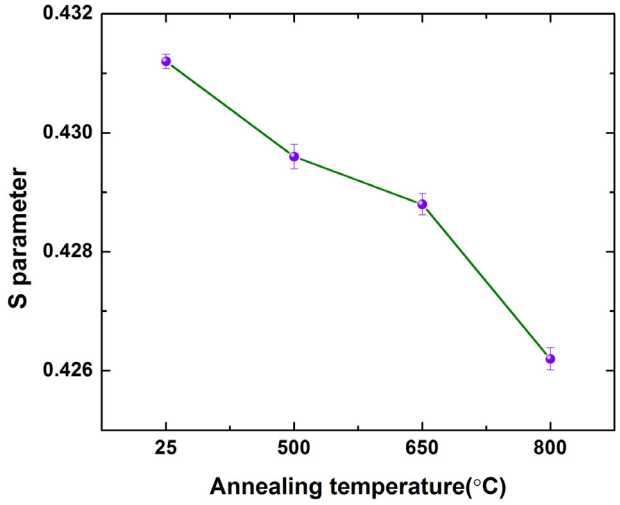

Fig. 4. The S-parameter as a function of the annealing temperatures for BFCTO samples.

Table 1
Positron lifetime results

Sample	τ1 (ps)	τ_2 (ps)	I_2 (%)	τ_m (ps)
BFCTO	233 (1.9)	427.7 (4.6)	26.57 (0.89)	284.7
BFCTO-500	239.9 (1.3)	447.5 (8.9)	15.42 (0.92)	271.9
BFCTO-650	227 (1.5)	415.2 (2.7)	14.08 (2.1)	253.5
BFCTO-800	218 (0.29)	408.8 (6.6)	9.03 (0.4)	232.0

3.3. Ferromagnetic behavior

Fig. 5a illustrates the magnetization versus applied magnetic field (M-H curves) of the BFCTO samples. We can observe from the defined M-H hysteresis loops that all the four samples clearly show ferromagnetism at RT. And it is also shown in Fig. 5b that with the increase of the annealing temperature, the saturation magnetization obviously decreases. We all know that magnetization could arise from very small clusters of magnetic dopants or impurities. In fact, the change of the saturation magnetization with annealing temperature could be due to a change in the amount of magnetic clusters. So it is necessary to consider the possibility of the presence of magnetic clusters or the impurities. In order to search for such problems, we employed TMG, TEM and mapping analysis to obtain the microstructural characteristics and the distribution of the elements in the sample. Fig. 6 shows the TMG curve with a 200 Oe applied magnetic field over a temperature range of RT to 970 K for BFCTO-RT. Only one peak temperature can be seen from the derivative weight (dW/dT) curve, which is located at 741.5 K. It suggests that there are no any other

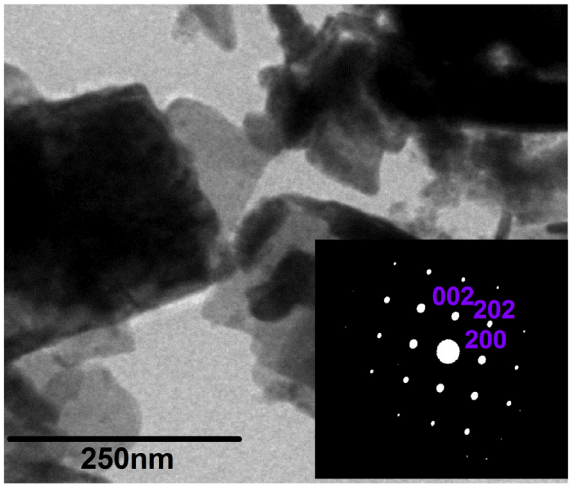

Fig. 7. TEM image of BFCTO-RT nanoplate, inset is a selected-area electron diffraction (SAED) pattern of BFCTO-RT.

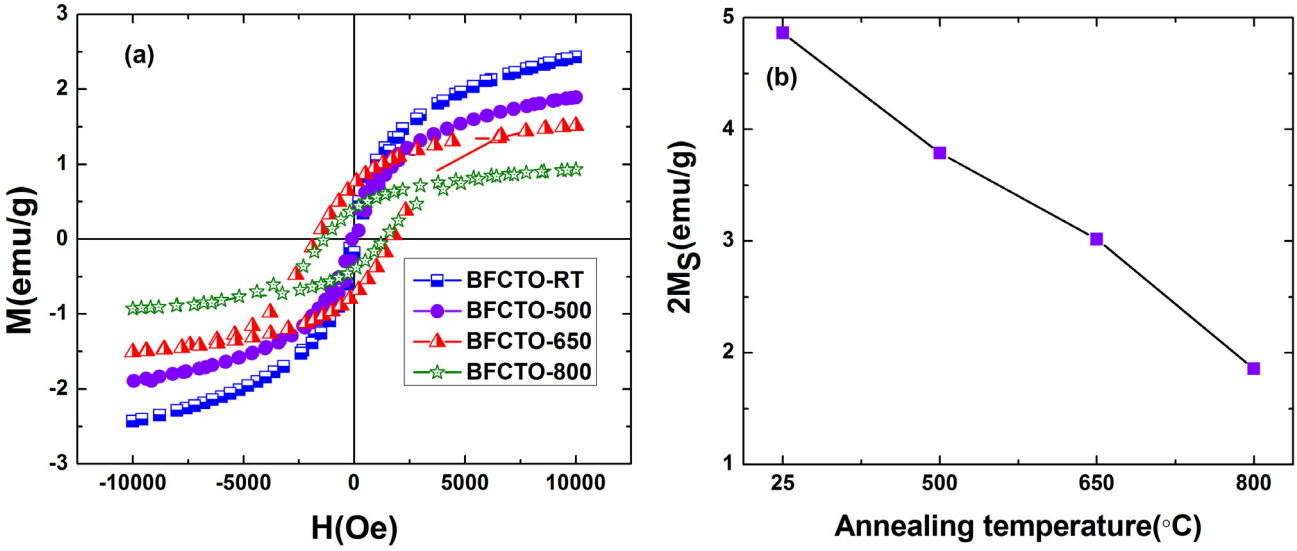

Fig. 5. (a) Magnetic hysteresis loops of BFCTO samples at RT. (b) The saturation magnetization as a function of the annealing temperatures for BFCTO samples.

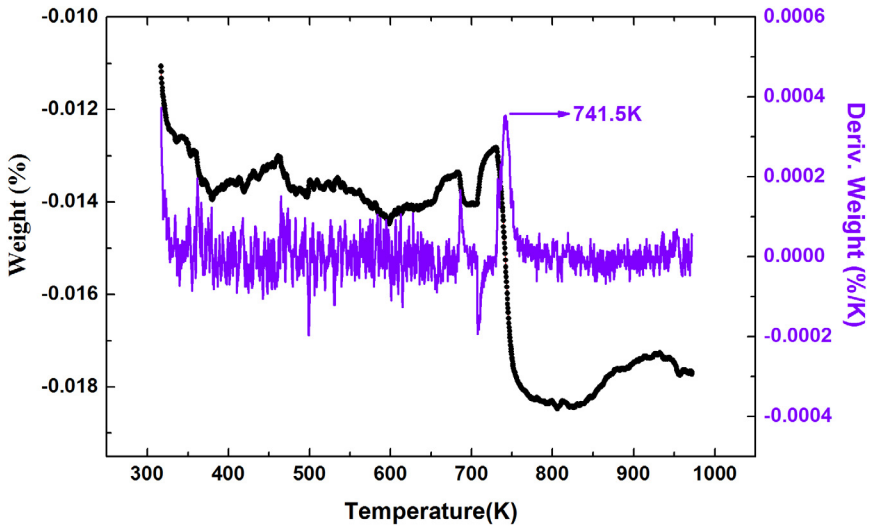

Fig. 6. Weight loss and DTMG curves of BFCTO-RT sample.

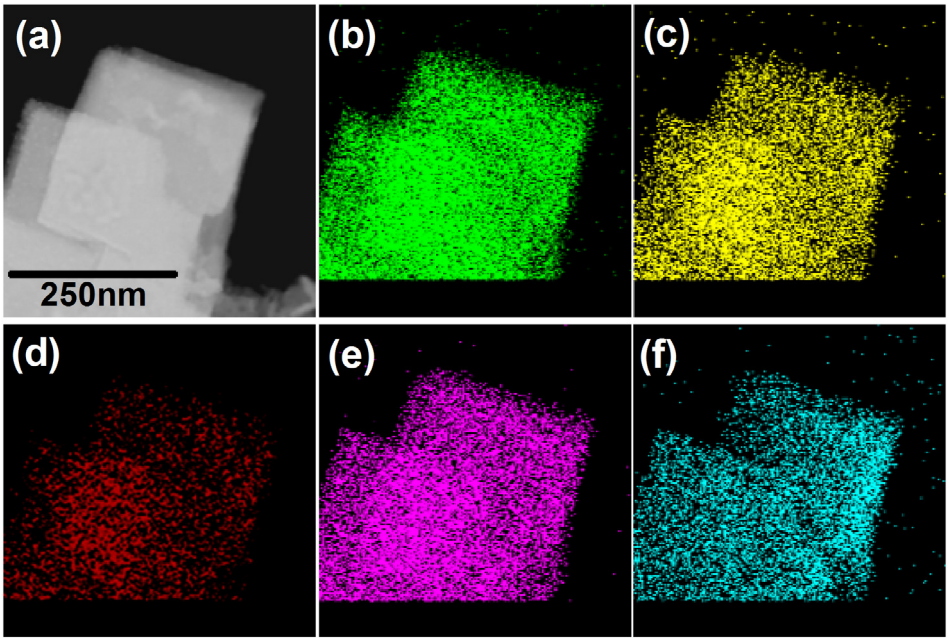

Fig. 8. STEM image and the corresponding EDS elemental mapping of the nanoplate-like BFCTO-RT (a) STEM, (b) Bi, (c) Fe, (d) Co, (e) Ti and (f) O elements.

impurities in the sample [33], which is consistent with the results of XRD. To further verify the single crystallinity, TEM image and a selected-area electron diffraction (SAED) pattern of BFCTO-RT were measured and shown in Fig. 7 and the inset. The sharp diffraction dots indicated good single crystallinity of the nanoplates. Fig. 8 displays the STEM image and the corresponding EDS elemental mapping of the BFCTO-RT sample. Homogeneous distribution of Bi, Fe, Co, Ti and O elements was observed in the nanoplate, which indicates that the Co ions are successfully doped into BFTO and no sign of Co aggregation is observed. Based on the analysis above, no evidence of other secondary phases or Co metal clusters is detected. It means that the saturation magnetization arises from the intrinsic properties instead of any impurities or small clusters of magnetic dopants in the BFCTO samples.

It is noted that the non-annealed sample has the highest saturation magnetization, and it also has the biggest value of mean lifetime, which means the concentration of the interfacial defects might quite be high and all of the positrons are trapped by these defects. After annealing at different temperatures, the saturation magnetization decreases obviously. At the same time, both the mean lifetime and S parameter decrease with the increase of annealing temperature, which means the interfacial defects have a gradual decrease with the increase of annealing temperature. Therefore, the variation of saturation magnetization in the BFCTO samples is consistent with the disappearance process of the interfacial defects, in other words, the results support the interfacial defects indeed playing a role in the ferromagnetism. It can be also inferred that the concentration of the interfacial defects is crucial to the saturation magnetization in the BFCTO samples. Though more comprehensive work should be done further, this work indeed provide an experiment reference of the relationship between interface and the magnetism.

4. Conclusion

In summary, we have studied the effect of annealing on the ferromagnetism and interfacial defects in the BFCTO samples. In the annealing temperature interval between 500 and 800 °C, no phase transition was observed. XRD patterns and TMG curve both confirm that all the samples are single phase with an Aurivillius structure. The results of the STEM image and element mapping of Bi, Fe, O, Ti and Co indicate that the Co ions are successfully doped into BFTO and no sign of Co aggregation is observed. The interfacial defects evidenced by positrons in the grain boundary region disappear slowly with the increase of annealing temperature. The magnetic measurements indicate that the saturation magnetization decreased with increasing the annealing temperature, which coincides with the variation of the concentration of interfacial defects, suggesting that the concentration of the interfacial defects can certainly effect the saturation magnetization. Our results clearly show a correlation between magnetic behavior and the positron response, which give important insight into the role of defects in magnetic properties and provide a new train of thought to improve the magnetism through controlling the concentration of interfacial defects.

Acknowledgments

This work was supported by the National Natural Science Foundation of China (Grant No. 11475165) and National Basic Research Program of China (2012CB922000).

References

[1] M. Fiebig, Revival of the magnetoelectric effect, J. Phys. D: Appl. Phys. 38 (2005) 123–152.
[2] W. Eerenstein, N.D. Mathur, J.F. Scott, Multiferroic and magnetoelectric materials, Nature 442 (2006) 759–765.
[3] S.-W. Cheong, M. Mostovoy, Multiferroics: a magnetic twist for ferroelectricity, Nat. Mater. 6 (2007) 13–20.
[4] X. Li, Z. Ju, F. Li, Y. Huang, Y. Xie, Z. Fu, R.J. Knized, Y. Lu, Visible light responsive $Bi_7Fe_3Ti_3O_{21}$ nanoshelf photocatalysts with ferroelectricity and ferromagnetism, J. Mater. Chem. A 2 (2014) 13366–13372.
[5] X. Li, Z. Zhu, F. Li, Y. Huang, X. Hu, H. Huang, R. Peng, X. Zhai, Z. Fu, Y. Lu, Multifunctional single-phase photocatalysts: extended near infrared photoactivity and reliable magnetic recyclability, Sci. Rep. 5 (2015) 15511.
[6] R. Ramesh, N.A. Spaldin, Multiferroics: progress and prospects in thin films, Nat. Mater. 6 (2007) 21–29.
[7] M. Krzhizhanovskaya, S. Filatov, V. Gusarov, P. Paufler, R. Bubnova, M. Morozov, D.C. Meyer, Aurivillius phases in the $Bi_4Ti_3O_{12}$/$BiFeO_3$ system: thermal behaviour and crystal structure, Z. Anorg. Allg. Chem. 631 (2005) 1603–1608.
[8] N.A. Lomanova, M.I. Morozov, V.L. Ugolkov, V.V. Gusarov, Properties of aurivillius phases in the $Bi_4Ti_3O_{12}$-$BiFeO_3$ system, Inorg. Mater. 42 (2006) 189–195.

[9] A. Kan, H. Ogawa, K. Kawada, T. Moriyama, Synthesis and ferroelectric properties of $Bi_{4.5}Sr_{0.5}Ti_4Fe_{0.5-x}V_xO_{15}$ ceramics, Ferroelectrics 427 (2012) 129–136.
[10] X. Mao, W. Wang, X. Chen, Y. Lu, Multiferroic properties of layer-structured $Bi_5Fe_{0.5}Co_{0.5}Ti_3O_{15}$ ceramics, Appl. Phys. Lett. 95 (2009) 082901.
[11] X. Li, Z. Zhu, F. Li, R. Peng, X. Zhai, Z. Fu, Y. Lu, Facile route to prepare grain-oriented multiferroic $Bi_7Fe_{3-x}Co_xTi_3O_{21}$ ceramics, J. Eur. Ceram. Soc. 35 (2015) 3437–3443.
[12] Z.-Y. Chen, Z.Q. Chen, D.D. Wang, S.J. Wang, Correlation between interfacial defects and ferromagnetism of $BaTiO_3$ nanocrystals studied by positron annihilation, Appl. Surf. Sci. 258 (2011) 19–23.
[13] J.B. Yi, C.C. Lim, G.Z. Xing, H.M. Fan, L.H. Van, S.L. Huang, K.S. Yang, X.L. Huang, X.B. Qin, B.Y. Wang, T. Wu, L. Wang, H.T. Zhang, X.Y. Gao, T. Liu, A.T. Wee, Y.P. Feng, J. Ding, Ferromagnetism in dilute magnetic semiconductors through defect engineering: Li-doped ZnO, Phys. Rev. Lett. 104 (2010) 137201.
[14] L. Balcells, J.I. Beltrán, C. Martínez-Boubeta, Z. Konstantinović, J. Arbiol, B. Martínez, Aging of magnetic properties in MgO films, Appl. Phys. Lett. 97 (2010) 252503.
[15] X.F. Liu, Y. Sun, R.H. Yu, Role of oxygen vacancies in tuning magnetic properties of Co-doped SnO_2 insulating films, J. Appl. Phys. 101 (2007) 123907.
[16] A. Sundaresan, R. Bhargavi, N. Rangarajan, U. Siddesh, C.N.R. Rao, Ferromagnetism as a universal feature of nanoparticles of the otherwise nonmagnetic oxides, Phys. Rev. B 74 (2006) 161306.
[17] A. Sundaresan, C.N.R. Rao, Ferromagnetism as a universal feature of inorganic nanoparticles, Nano Today 4 (2009) 96–106.
[18] X. Zhu, R. Birringer, U. Herr, H. Gleiter, X-ray diffraction studies of the structure of nanometer-sized crystalline materials, Phys. Rev. B 35 (1987) 9085–9090.
[19] R. Krause-Rehberg, H.S. Leipner, Positorn Annihilation in Semiconductors, Defect Studies, Springer Series in Solid-State Sciences, vol. 127, Springer, Berlin, 1999.
[20] S. Chakraverty, S. Mitra, K. Mandal, P.M.G. Nambissan, S. Chattopadhyay, Positron annihilation studies of some anomalous features of $NiFe_2O_4$ nanocrystals grown in SiO_2, Phys. Rev. B 71 (2005) 024115.
[21] R.M. Nieminen, M.J. Manninen, Positrons in Solids, Springer, Berlin, 1979, pp. 145–195.
[22] H.-E. Schaefer, R. Wurschum, R. Birringer, H. Gleiter, Structure of nanometer-sized polycrystalline iron investigated by positron lifetime spectroscopy, Phys. Rev. B 38 (1988) 9545.
[23] C.H. Shek, J.K.L. Lai, G.M. Lin, Investigation of interface defects in nanocrystalline SnO_2 by positron annihilation, J. Phys. Chem. Solids 60 (1999) 189.
[24] J. Kuriplach, Positron-defect interactions in complex systems, Appl. Surf. Sci. 194 (2002) 61.
[25] S. Chakrabarti, S. Chaudhuri, P.M.G. Nambissan, Positron annihilation lifetime changes across the structural phase transition in nanocrystalline Fe_2O_3, Phys. Rev. B 71 (2005) 064105.
[26] A.K. Mishra, S.K. Chaudhuri, S. Mukherjee, A. Priyam, A. Saha, D. Das, Characterization of defects in ZnO nanocrystals: photoluminescence and positron annihilation spectroscopic studies, J. Appl. Phys. 102 (2007) 103514.
[27] T. Ghoshal, S. Biswas, S. Kar, S. Chaudhuri, P.M.G. Nambissan, Positron annihilation spectroscopic studies of solvothermally synthesized ZnO nanobipyramids and nanoparticles, J. Chem. Phys. 128 (2008) 074702.
[28] S. Dutta, S. Chattopadhyay, D. Jana, A. Banerjee, S. Manik, S.K. Pradhan, M. Sutradhar, A. Sarkar, Annealing effect on nano-ZnO powder studied from positron lifetime and optical absorption spectroscopy, J. Appl. Phys. 100 (2006) 114328.
[29] D. Sanyal, D. Banerjee, Probing $(Bi_{0.92}Pb_{0.17})_2Sr_{1.91}Ca_{2.03}Cu_{3.06}O_{10+\delta}$ superconductors from 30 to 300 K by positron-lifetime measurements, Phys. Rev. B 58 (1998) 15226–15230.
[30] M. Mukherjee, D. Chakravorty, Annihilation characteristics of positrons in a polymer containing silver nanoparticles, Phys. Rev. B 57 (1998) 848–856.
[31] H.Y. Tong, B.Z. Ding, J.T. Wang, K. Lu, J. Jiang, J. Zhu, Investigations spectroscopy on nanocrystalline $Fe_{78}B_{13}Si_9$ alloys by positron annihilation, J. Appl. Phys. 72 (1992) 5124–5129.
[32] P.P. Chattopadhyay, P.M.G. Nambissan, S.K. Pabi, I. Manna, Polymorphic bcc to fcc transformation of nanocrystalline niobium studied by positron annihilation, Phys. Rev. B 63 (2001) 054107.
[33] S. Sun, Y. Huang, G. Wang, J. Wang, Z. Fu, R. Peng, R.J. Knize, Y. Lu, Nanoscale structural modulation and enhanced room-temperature multiferroic properties, Nanoscale 6 (2014) 13494–13500.